Corrosion and depassivation of a chromia-forming Ni-based alloy in the 0.75Na2O-B2O3-2.75SiO2 melt

V. Szczepan, C. Petitjean, P.J. Panteix, M. Vilasi

Corrosion and depassivation of a chromia-forming Ni-based alloy in the $0.75Na_2O$-B_2O_3-$2.75SiO_2$ melt

V. Szczepan[1], C. Petitjean[1], P.J. Panteix[1], M. Vilasi[1]

[1]Université de Lorraine, CNRS, IJL, F-54000 Nancy, France

Abstract

Corrosion resistance of nickel based alloys in **molten silicates** is linked to the temperature. Above a certain temperature, the protection of the alloy by a chromia layer is no more ensured: this depassivation phenomenon leads to active corrosion. Electrochemical methods were used for *in situ* characterization, and Scanning Electron Microscopy (SEM) and Scanning Electron Transmission Microscopy (STEM) were used in order to measure the oxide thickness after immersion. Corrosion tests with increasing temperature showed that above a certain temperature, the oxide thickness decreased homogeneously leading to the depassivation of the alloy. The different steps of this phenomenon are discussed here.

Keywords

High temperature corrosion, depassivation, Ni-based alloy, chromia-forming alloy, corrosion potential.

1. Introduction

Contact between alloys and molten silicates based glasses are encountered in many industrial applications, for instance, in the production of glass fiber [1,2] or for the vitrification of nuclear wastes [3]. Nickel-based or cobalt-based chromia forming alloys are widely used in these applications due to theirs good mechanical properties at high temperature and their ability to develop a protective chromia layer [4].

In order to enhance the protective behavior of chromia-forming nickel-based alloys, a pre-oxidation step is performed to form a passivating chromia layer before immersion. Lizarazu noticed that a nickel based alloy with 30% mass of chromium (noted here as Ni-30Cr) exhibits a better corrosion resistance after two hours of immersion at 1100 °C when pre-oxidized 35 min in air at 1100 °C instead of being directly immersed [5]. Pre-oxidation was **then commonly** used for corrosion resistance studies [6,7]. The efficiency of the pre-oxidation is explained by the compactness of the chromia layer formed by oxidation in air as well as the low solubility of chromia in molten silicates [8], which induces a limited recession of the passive layer and thus confers its protective properties against high temperature corrosion by molten silicates [9–11]. The knowledge of the conditions of stability of this protective oxide layer is the key to predict the corrosion rate of the material and thus its durability.

Electrochemical methods can help to study this subject. First, these methods can be used in silica-based liquids due to the high ionic conductivity of these media. **Second**, as these methods are *in situ* measurements, they give access to corrosion properties of materials in conditions. As an example, corrosion potential measurements give information about the corrosion state of the material i.e. passive or active [1,2]. Moreover, the results are not subject to deterioration by quenching or polishing as for electronic microscopy characterization.

Among the previous works dealing with the corrosion study of nickel based alloys by silica-based liquids, some of them studied and highlighted the importance of temperature on the stability of the chromia layer. Carton *et al.* [7] proposed an experimental procedure in which the temperature is slowly increased at 5°C/h and 10°C/h while the pre-oxidized alloy is immersed in the liquid. Corrosion potential measurements showed that above a certain temperature, the chromia layer stops to ensure its protective properties and is dissolved by the melt. This phenomenon was called depassivation and its origin is not understood but it seems to appear in various kinds of silicates, e.g. soda-lime-silicates [6] and boro-silicates [12].

In the experimental procedure proposed by Carton *et al.* [7], the influence of parameters such as pre-oxide thickness, immersion temperature or temperature increase rate was not verified. In their works, Schmucker *et al*. had shown that the formation of the oxide occurs continuously during the immersion [12]. As a consequence, a slow temperature increase rate involves a longer time immersion, and thus a significant increase of the oxide thickness during immersion.

In the present work the depassivation of Ni-30Cr alloy in a ternary Na_2O-B_2O_3-SiO_2 was studied. **The selected glass composition was 0.75Na_2O-B_2O_3-2.75SiO_2 (0.75NB2.75S) which was first formulated as a model nuclear glass** [13]. Various values of the temperature increase rate, the pre-oxide thickness and the starting immersion temperature were tested in order to optimize the experimental procedure. *Ex situ* characterization (Scanning Electron Microscopy SEM and Scanning Transmission Electron Microscopy STEM) coupled with *in situ* electrochemical measurements were used in order to characterize the oxide layer during the depassivation. These are the first observations of alloys subject to this phenomenon reported in the literature to our knowledge.

2. Materials and methods

2.1. Alloy and glasses synthesis

Ni-30Cr alloy was elaborated by high frequency induction melting in neutral atmosphere (argon O_2 < 2 ppm). Ingots of 40 – 50 g were melted from pure chromium (Alfa Aesar chromium pieces, 3 – 8 mm (0.1 - 0.31 in), 99.99%) and pure nickel (Alfa Aesar nickel shot, 3 – 25 mm (0.1 - 0.98 in), 99.95%). Two melting steps were performed to ensure compositional homogeneity. Then, molten ingots were aspirated into silica pipes (inner diameter: 6 mm, length: 150 mm) using a primary vacuum pump. This device allows a slow quenching of the alloy giving time for an important grain growth. Thus, the rods microstructure presents grains of several hundreds (up to several thousands) micrometers. Rods were cut and shaped to obtain suitable dimensions (diameter: 5.5 mm, length: 25 mm). They were then ground with P1200 SiC paper for reproducible surface condition and ultrasonically cleaned in absolute ethanol.

Glass was elaborated by the CERFAV (Centre Européen de Recherche et de Formation aux Arts Verriers). SiO_2, Na_2CO_3 and H_3BO_3 powders were mixed and heated at high temperature to obtain homogenous liquids. The low sodium concentration limits the volatilization of that element from the melt and ensures the stability of the composition during

long time exposure at high temperature [14]. Composition was controlled by EPMA, results are available in ref [13]. Acid-base properties of the silica-based liquids are expressed in the well-known concept of optical basicity [15]. With a value of 0.52 this glass is more acidic than common nuclear glasses. Viscosity of the melt was calculated using the Factsage software [16]. A value close to the one corresponding to the R7T7 nuclear glass was found (117 dPa.s for 0.75NB2.75S and 157 dPa.s for R7T7 at 1150°C [12]).

2.2. Corrosion measurements

Corrosion potential (*i.e* open circuit potential) of alloys was measured during immersion. A classical three electrodes device was adapted to high temperature molten silicates. This device was described elsewhere [1,2]. Working electrode was made of Ni-30Cr, counter electrode was a platinum plate and reference electrode was an yttria stabilized zircona (YSZ) stick. A platinum wire (diameter: 0,5 mm) was welded to rod to ensure electrical conductivity across mullite tube; in the case of reference electrode, platinum lacquer was used as junction between ceramic and platinum wire. Electrodes were sealed in mullite tubes with alumina cement (Resbond 989FS).

2.3. Immersion procedure

Immersion tests of Ni-30Cr alloys were performed at high temperature. The following procedure was used in order to study depassivation phenomenon. 600 g of pieces of the studied glass were placed in a Pt-10%Rh crucible (inner diameter: 115 mm, depth: 80 mm) and molten in a furnace **in air**; temperature was increased to 1150 °C in 2 hours, maintained at 1150 °C for 10 min and decreased to room temperature in 2 hours. Then Ni-30Cr electrode was placed in the furnace above the molten silicate bath and heated at 942 °C for 64 hours. It was thus pre-oxidized **in air** in order to obtain an initial chromia layer with an expected thickness of 2 µm. The working, counter and reference electrodes were immersed at the end of the pre-oxidation time. Corrosion potential of the working electrode was measured during immersion; temperature was increased at a constant rate of 50°C/h until the measured potential fell down to active state (< -1000 mV/Ref **above 1000 °C**) [13]. Temperature was measured in the liquid with an S-type thermocouple (Pt/Pt-10Rh) during the experiment to be sure of the thermal equilibrium in the liquid. Ni-30Cr working electrode was then quenched and embedded in resin. All the immersion procedure is summarized in figure 1.

Three parameters can be adjusted in this experiment: pre-oxidation duration (and thus the initial oxide thickness), temperature increase rate and initial immersion temperature. Two pre-oxidation durations of 64 h and 16 h were tested at 942 °C. Due to the well-known

parabolic growth of chromia layer on alloys at high temperature [4,17–19], the thickness of the pre-oxidized layer is two times lower after 16 h than after 64 h of oxidation. Temperature increase rates from 10 °C/h up to 150 °C/h and immersion temperature from 890 °C to 1018 °C were also tested.

2.4. Electronic microscopy characterization

2.4.1. Metallographic preparation

After quenching, rods were embedded in resin and cut in order to realize cross section characterizations of glass/oxide/alloy interface. Samples were polished using SiC paper (grid P120 to P1200), then with diamond gel (9 µm to 1 µm) and finally OPS (colloidal suspension of amorphous silica 40 nm). Embedded samples were ultrasonically cleaned in absolute ethanol.

2.4.2. SEM and STEM analysis

Scanning electron microscopy was performed with a JEOL 6010LA at an acceleration voltage of 15 kV and a current beam of 6 nA in Back Scattered Electron (BSE) mode to obtain a compositional contrast. The apparatus is equipped with an Energy Dispersion Spectrometer (EDS) to get information about the elemental composition of the sample. Gold metallization was carried out with aim to avoid polarization of the non-conducting surface. Gold was chosen due to its high electronic conductivity providing good micrograph quality. **The thicknesses of the oxide layers were measured specifically on non-deteriorated areas of the sample (no cracks or unsticking of the glass/oxide interface) to ensure the reliability of the results. The average oxide thickness of a sample was calculated from 10 to 15 measurements, and the uncertainty is evaluated as the standard deviation**.

In order to perform scanning transmission electron microscopy analysis, a thin slice (**10 × 2 × 0.2 µm**) of the glass/alloy interface was extracted from in the analyzed sample using a scanning electron microscope coupled with a focused ion beam (FIB) (Helios Nanolab 600i FEI). STEM was performed with a JEOL ARM 200F TEM in STEM mode **using the HAADF (dark field) detector for imaging** with an acceleration tension of 200 kV and EDS detector for elemental analysis. **The electron beam focus on the sample in STEM mode allows probing an area of 1 nm in diameter and 200 nm in depth (across the thin slice).**

3. Results and discussions

3.1. Immersion and characterization

3.1.1. Features of the corrosion potential

Electrochemical measurements were performed in the reference silica-based liquid. The procedure described in the previous section was applied with a pre-oxidation duration of 64 h at 942 °C, an immersion temperature of 942 °C and a temperature increase rate of 50 °C/h.

Figure 2 shows the evolution of the corrosion potential of the alloy versus the temperature. The curve is monotonously decreasing and can be divided in three parts. A first smooth part **(I)** extending from the immersion to a temperature around 1150 °C; a second rough part **(II)** from 1150 °C to 1230 °C and a third part **(III)** above 1230 °C. The first two parts can be differentiated by a change of aspect but the values of the potential between 0 and -1000 mV/ref indicate that the alloy is in the passive state in these two first stages [13]. The temperature of 1230°C is characterized by a clear potential drop which leads to an active potential implying a loss of the protective oxide layer.

3.1.2. SEM and STEM characterization of the sample

Since the corrosion potential of the alloy versus the temperature varies in a specific way, other measurements of the corrosion potential of the Ni-30Cr alloy in the 0.75NB2.75S liquid were performed. Samples were quenched at specific moments according to the shape of the potential curve, and characterized by SEM.

Potential measurements of those samples are presented in figure 3; the potential curves exhibit the same decreasing trend. The quenched samples are represented by black dots, the corresponding oxide thicknesses are represented by the red squares. The SEM micrographs are presented in figure 4. The micrograph (a) corresponds to the pre-oxidized sample immersed for one minute. The thickness of the pre-oxide is 2.4 ± 0.7 µm, oxide needles can be noticed on the sample which is characteristic of dissolution/precipitation of the oxide. As for the corrosion potential curve, the evolution of the thickness can be divided in three parts. A first decreasing part characterized by micrographs **(a), (b) and (c)** with a covering oxide layer inhomogeneous in thickness which corresponds to the part I of the potential curve. Oxide needles can be observed on these samples. In the second part corresponding to the micrograph **(d)**, the oxide thickness increases and the oxide layer becomes thicker than the initial pre-oxidized sample. The last part corresponds to micrographs **(e) and (f)**. A clear decrease of the oxide thickness can be noticed, this one leading to a complete loss of the oxide

layer. The standard deviation of thickness measurements decreases with the immersion duration in figure 3, which can be a sign of the formation and dissolution of the oxide layer: as both phenomena are diffusion controlled, the heterogeneities of the layer are smoothed during the long time immersions.

These variations of the oxide thickness are interpreted as follows:

- During the first moments of immersion, the formation of the oxide is limited by its own thickness [17] while the absence of chromium in the liquid generates a high concentration gradient of chromium. Schmucker *et al.* assumed that the dissolution is limited by the diffusion of chromium in the liquid [13]. In this case the high chromium gradient involves a fast dissolution rate overcoming the formation rate. This leads to a loss of the oxide thickness (Figure 4b and 4c). Thus, the first part of the immersion corresponds to a light dissolution of the oxide layer.

- The dissolution rate decreases with immersion time because of the flattening of the concentration profile of chromium in the liquid with time [20]. A regime of formation slowed down by the dissolution takes place and yields a **light** increase of the oxide thickness **(Figure 4d)**. **Indeed, in previous works, when the temperature is lower than the depassivation temperature, a significant increase of the thickness of the oxide layer is observed. For example [6], the thickness of the chromia layer of a pre-oxidized Ni-30Cr sample immersed in a soda-lime silicate at 1100°C increases from 4 µm to 10 µm in 24 h. Consequently, we can expect an increase of the thickness of the chromia layer in the low temperature range.** Furthermore, at higher temperature the growth rate of the protective layer becomes important in comparison to its dissolution due to a parabolic growth constant of the oxide increasing faster [4] than the dissolution rate [11,16] with the temperature.

- The oxide thickness decreases on the sample (e) which was quenched just before the final potential falls down to the active state. This means that the formation/dissolution competition is overcome by dissolution. The protective layer is no longer present on sample (f), which concords with the very low potential of this sample.

Two hypotheses can be proposed to explain the last point: either the dissolution of the chromia layer, or the formation rate become respectively greater and lower than expected from the extrapolation of lower temperature values. For the first hypothesis, data on solubility and diffusion of chromium in molten silicates, so as silica-based liquids viscosity are pretty well known [10,11,13,21,22]. In each case, an Arrhenius type law describes the evolution of these parameters with temperature. No deviation from these behaviors was reported. Regarding the second hypothesis, a lack of the oxygen (O_2) supply towards the growing oxide layer could decrease the formation rate of the oxide by hampering its oxidation, and thus lead to a complete loss of the passivating layer. This explanation has already been proposed to explain the low corrosion resistance of chromia-forming alloys in molten silicates in argon atmosphere [23]. Activity measurements of the oxygen (O_2) in silica-based liquids have been reported in the literature [24], but the link between such measurements and the concentration of dissolved oxygen has not been established yet. The origin of depassivation cannot be clearly defined due to the lack of data on the dissolved oxygen.

As expected, the selective oxidation of chromium leads to a pronounced concentration gradient over several tens of microns. The depassivated sample (f) was also analyzed by STEM. Composition of the alloy was checked close to the glass/alloy interface using an EDS detector **coupled with STEM**. The analyzed area and the concentration profiles are presented in figure 5 and 6 respectively. Each concentration profile **appears flat due to the high magnification**. Silicon was detected at about 2 at.% in the alloys with an homogeneous distribution over the 600 nm of analysis. The presence of this element near the interface has already been observed by Abdullah *et al.* [6] and can be attributed to the diffusion of metallic silicon produced by reduction of silica from the liquid. The formal potentials of different elements were studied by Petitjean *et al.* [25]. The potential of Si^{VI}/Si^0 couple is around -1150 mV/(YSZ reference electrode) in silica-based liquids **above 1000 °C**. The corrosion potential of a depassivated Ni-30Cr alloy is lower than this value (< -1200 mV/ref) involving that the reduction of silica is thermodynamically allowed. Moreover, the formal potential of Cr^{II}/Cr^0 in these media **and in this range of temperature** is around -1300 mV/ref. So, silica is a strong enough oxidant to be reduced by chromium on the surface of the alloy according to the following reaction.

$$2Cr^0_{(alloy)} + Si^{IV}_{(liquid)} \Rightarrow 2Cr^{II}_{(liquid)} + Si^0_{(alloy)} \quad (1)$$

Thus, this reaction leads to Cr^{II} in the liquid and Si^0 in the **Ni-Cr CFC solid solution**. Usually, the main oxidant compound in the melt is the oxygen (O_2) which is a strong enough oxidant to oxidize Cr^0 in Cr_2O_3. The reaction of chromium and silica involves a low oxygen activity at the liquid/alloy interface which is in agreement with the lack of oxygen supply stated in the previous section.

The diffusion profiles of chromium and nickel (figure 6) show a concentration gradient of nickel with a negative value from the bulk to the interface. This involves a diffusion of the nickel towards the liquid/oxide interface and so a consumption of this element by the corrosion process of the depassivated alloy. Nickel was detected in the glass by EDS analysis so as chromium which confirms the consumption of this two element during the active corrosion process. Nickel in the glass and silicon in the alloy were not detected in the passivated samples.

3.2. Parameters influencing the depassivation

3.2.1. Temperature increase rate

Four experiments were performed with the following temperature increases rates: 10, 50, 75, 150 °C/h and unchanged pre-oxidation conditions (942 °C during 64 h). Potential curves are shown in figure 7. The curves exhibit the same trend of the potential evolution in these conditions. At a temperature above 1150 °C, two behaviors appear. The corrosion potential of the sample heated at 10 °C/h falls down to -800 mV/ref, which corresponds to the passive state range of Ni-30Cr [13]. SEM micrograph confirms this result as shown in figure 8: a homogeneous oxide thickness (11.8 ± 1.7 µm) was formed probably due to the long immersion duration before the critical temperature of depassivation. The potential peaks at the end of this curve were identified as being due to the penetration of the molten silicate into the YSZ reference electrode which alters the measured potential. For 50, 75 and 150 °C/h the corrosion potential decreases faster to a value below -1200 mV/ref which is typical of the active state [13]. A same depassivation temperature of 1240 ± 10 °C was measured in these three cases. SEM analysis confirms the absence of the oxide layer on this sample. These faster temperature increase rates correspond to relatively shorter immersion time (3-7 hours) compared to 10 °C/h (40 hours of immersion), so the oxide growth is limited, leading to the same depassivation temperature. Moreover, the shape of the potential curve is similar for 50, 75 and 150 °C/h indicating the depassivation is more related to temperature and oxide thickness than to immersion duration. The reason of this better behavior during the slow

temperature increase would probably be related to the better relaxation of the expansion constrain at the alloy/oxide interface.

3.2.2. Pre-oxide thickness

Pre-oxidation duration was 16 and 64 h at a temperature of 942 °C. Pre-oxide thicknesses were measured by SEM analysis. The oxide thicknesses were 1.3 ± 0.2 µm and 2.4 ± 0.7 µm (section *3.1.2.*) for 16 h and 64 h respectively. Immersions were performed for these two pre-oxidation conditions with the following parameters: temperature increase rate of 50 °C/h and immersion temperature of 942 °C. Potential curves for these two conditions are presented in figure 9. Depassivation temperature is lower for the 16 h pre-oxidized sample than for the 64 h (1200 °C and 1235 °C respectively). This is coherent with the conclusion of the previous section: depassivation phenomenon is strongly linked to oxide thickness and its evolution during the immersion. It is also possible to state that the depassivation is initiated in a temperature range lightly below 1200°C.

3.2.3. Immersion temperature

In the section *3.1.2*, evidences that the depassivation occurs above a specific temperature were found. In order to confirm that assumption, different immersion temperatures were tested. As previously, the other conditions were fixed in order to isolate the influence of the immersion temperature. Pre-oxidation temperature and duration were 942 °C and 64 h respectively, temperature increase rate was 50 °C/h. At the end of the pre-oxidation, temperature was adjusted to reach 890 °C or 1018 °C. This step was quickly achieved (less than 10 min) and the oxide thickness was assumed to not be affected during this duration. Results of the corrosion potential measurements for these three immersion temperatures are shown in figure 10. The depassivation appears in a restricted temperature range (1250 ± 20 °C). Moreover, these values are close to those obtained with different temperature increase rates (i.e. 1240 ± 10 °C for 50, 75, 150 °C/h). No relation was found between immersion temperature and depassivation temperature implying that the depassivation does not occur between 890 °C and 1018 °C in this silica-based liquid.

4. Conclusion

In this paper, the corrosion of a chromia forming alloy was studied by considering the influence of temperature, pre-oxide thickness. An experimental procedure, based on the tests of the previous studies, was proposed. Corrosion potential measurements of the immersed alloy with a fast increase of the temperature allowed studying the depassivation phenomenon

over a wide range of temperature. By coupling electrochemical measurements to post-immersion SEM and STEM characterizations, a mechanism of the depassivation of the chromia forming alloy was proposed. At low temperature the formation is predominant on dissolution leading to an increase of the oxide thickness, whereas at high temperature the dissolution becomes predominant leading to a fast decrease of the oxide thickness until its complete dissolution and an active corrosion of the alloy. Then, silica becomes the main oxidant species which was proved by the presence of silicon in the alloy detected by EDS analysis. Thanks to SEM characterization, it has been shown that depassivation starts before the final potential fall down. Different experimental parameters were varied. From these tests, it had been shown that depassivation is strongly linked to the oxide thickness and its evolution during the immersion. The origins of the depassivation are still debated but this phenomenon is likely due to a decrease of the formation rate of the oxide in the liquid at high temperature. **However, the duration required to complete the depassivation might be affected the viscosity of the liquid and the solubility of chromium. As these parameters are linked to the Na_2O and B_2O_3 contents, the glass composition might also have an influence on the depassivation phenomenon.**

Acknowledgements

The authors wish to thank the « Centre de Compétences en Microscopies, Microsondes et Métallographie » of the Jean Lamour institute for providing the technical support for the FIB/STEM analysis presented in this work.

References

[1] J. Di Martino, C. Rapin, P. Berthod, R. Podor, P. Steinmetz, Corrosion of metals and alloys in molten glasses. Part 1: glass electrochemical properties and pure metal (Fe, Co, Ni, Cr) behaviours, Corros. Sci. 46 (2004) 1849–1864. https://doi.org/10.1016/j.corsci.2003.10.024.

[2] J. Di Martino, C. Rapin, P. Berthod, R. Podor, P. Steinmetz, Corrosion of metals and alloys in molten glasses. Part 2: nickel and cobalt high chromium superalloys behaviour and protection, Corros. Sci. 46 (2004) 1865–1881. https://doi.org/10.1016/j.corsci.2003.10.025.

[3] P. Sengupta, Interaction study between nuclear waste-glass melt and ceramic melter bellow liner materials, J. Nucl. Mater. 411 (2011) 181–184. https://doi.org/10.1016/j.jnucmat.2011.01.122.

[4] E. Schmucker, C. Petitjean, L. Martinelli, P.-J. Panteix, S. Ben Lagha, M. Vilasi, Oxidation of Ni-Cr alloy at intermediate oxygen pressures. I. Diffusion mechanisms through the oxide layer, Corros. Sci. 111 (2016) 474–485. https://doi.org/10.1016/j.corsci.2016.05.025.

[5] D. Lizarazu, Comportement en oxydation à l'air et comportement électrochimique dans le verre fondu d'alliages nickel-chrome, Thesis, Univerité de lorraine, Nancy, 1997.

[6] T.K. Abdullah, C. Petitjean, P.J. Panteix, E. Schmucker, C. Rapin, M. Vilasi, Corrosion of Pure Cr and Ni–30Cr Alloy by Soda–Lime–Silicate Melts: Study of Simplified Systems, Oxid. Met. 85 (2016) 3–16. https://doi.org/10.1007/s11085-015-9571-2.

[7] A. Carton, C. Rapin, R. Podor, P. Berthod, Corrosion of Chromium in Glass Melts, J. Electrochem. Soc. 153 (2006) B121. https://doi.org/10.1149/1.2165745.

[8] L.J. Manfredo, R.N. McNally, Solubility of Refractory Oxides in Soda-Lime Glass, J. Am. Ceram. Soc. 67 (1984) C–155–C–158. https://doi.org/10.1111/j.1151-2916.1984.tb19178.x.

[9] C.-W. Kim, K. Choi, J.-K. Park, S.-W. Shin, M.-J. Song, Enthalpies of Chromium Oxide Solution in Soda Lime Borosilicate Glass Systems, J. Am. Ceram. Soc. 84 (2001) 2987–2990. https://doi.org/10.1111/j.1151-2916.2001.tb01125.x.

[10] H. Khedim, R. Podor, C. Rapin, M. Vilasi, Redox-Control Solubility of Chromium Oxide in Soda-Silicate Melts, J. Am. Ceram. Soc. 91 (2008) 3571–3579. https://doi.org/10.1111/j.1551-2916.2008.02692.x.

[11] H. Khedim, R. Podor, P.J. Panteix, C. Rapin, M. Vilasi, Solubility of chromium oxide in binary soda-silicate melts, J. Non-Cryst. Solids. 356 (2010) 2734–2741. https://doi.org/10.1016/j.jnoncrysol.2010.09.045.

[12] T.K. Abdullah, Study of the redox and acid-base properties of soda-lime silicate glass : appliacation to the high temperature corrosion of the Ni-based alloys and ceramic materials, Thesis, Univerité de lorraine, Nancy, 2013.

[13] E. Schmucker, C. Petitjean, P.-J. Panteix, L. Martinelli, S. Ben Lagha, M. Vilasi, Correlation between chromium physicochemical properties in silicate melts and the corrosion behavior of chromia-forming alloy, J. Nucl. Mater. 510 (2018) 100–108. https://doi.org/10.1016/j.jnucmat.2018.07.059.

[14] M. Cable, Kinetics of Volatilization of Sodium Borate Melts, in: L.D. Pye, V.D. Fréchette, N.J. Kreidl (Eds.), Borate Glas., Springer US, Boston, MA, 1978: pp. 399–411. http://link.springer.com/10.1007/978-1-4684-3357-9_20 (accessed September 30, 2019).

[15] J.A. Duffy, A review of optical basicity and its applications to oxidic systems, Geochim. Cosmochim. Acta. 57 (1993) 3961–3970. https://doi.org/10.1016/0016-7037(93)90346-X.

[16] C.W. Bale, E. Bélisle, P. Chartrand, S.A. Decterov, G. Eriksson, K. Hack, I.-H. Jung, Y.-B. Kang, J. Melançon, A.D. Pelton, C. Robelin, S. Petersen, FactSage thermochemical software and databases — recent developments, Calphad. 33 (2009) 295–311. https://doi.org/10.1016/j.calphad.2008.09.009.
[17] C. Wagner, Beitrag zur Theorie des Anlaufvorgangs, Z. Für Phys. Chem. 21B (1933). https://doi.org/10.1515/zpch-1933-2105.
[18] G.M. Ecer, G.H. Meier, Oxidation of high-chromium Ni-Cr alloys, Oxid. Met. 13 (1979) 119–158. https://doi.org/10.1007/BF00611976.
[19] T. Ramanarayanan, Transport through chromia films, Solid State Ionics. 136-137 (2000) 83–90. https://doi.org/10.1016/S0167-2738(00)00355-6.
[20] J. Crank, The mathematics of diffusion, Oxford university press, 1979.
[21] T.K. Abdullah, C. Petitjean, P.-J. Panteix, C. Rapin, M. Vilasi, Z. Hussain, A. Abdul Rahim, Dissolution equilibrium of chromium oxide in a soda lime silicate melt exposed to oxidizing and reducing atmospheres, Mater. Chem. Phys. 142 (2013) 572–579. https://doi.org/10.1016/j.matchemphys.2013.07.055.
[22] A. Fluegel, Glass viscosity calculation based on a global statistical modelling approach, Glass Technol.-Eur. J. Glass Sci. Technol. Part. 48 (2007) 13–30.
[23] B. Gaillard Allemand, Etude de la corrosion de materiaux metalliques et ceramiques par le verre de confinement des dechets nucleaires fondu, Thesis, Universite de lorraine, Nancy, 2001.
[24] C. Rüssel, R. Kohl, H.A. Schaeffer, Interaction between oxygen activity of Fe2O3 doped soda-lime-silica glass melts and physically dissolved oxygen, 61 (1988) 209–213.
[25] C. Petitjean, P.J. Panteix, C. Rapin, M. Vilasi, R. Podor, Electrochemical Behavior of Glass Melts: Application to Corrosion Processes, Procedia Mater. Sci. 7 (2014) 101–110. https://doi.org/10.1016/j.mspro.2014.10.014.

Figure captions

Fig 1. Pre-oxidation and immersion procedure of Ni-30Cr (working electrode).

Fig 2. Corrosion potential of Ni-30Cr vs temperature in 0.75NB2.75S. Pre-oxidation: 64h at 942°C; immersion temperature: 942°C; temperature increase rate: 50°C/h.

Fig 3. Corrosion potential of pre-oxidized Ni-30Cr (64 h at 942 °C) vs temperature in 0.75NB2.75S (50 °C/h) for various quenching (**black dots**) and corresponding oxide thickness (**red squares**).

Fig 4. SEM micrographs of Ni-30Cr alloys corresponding to quenched samples in figure 3.

Fig 5. STEM micrograph in dark field mode of the glass/alloy interface on a depassivated Ni-30: sample (f).

Fig 6. Concentration profiles of nickel, chromium and silicon in the alloy vs the distance from the glass/alloy interface on the depassivated sample (f).

Fig 7. Corrosion potential of pre-oxidized Ni-30Cr vs the temperature in 0.75NB2.75S for various temperature increases rates. Pre-oxidation: 64h at 942°C.

Fig 8. SEM micrograph of Ni-30Cr pre-oxidized at 942°C for 64h and immersed in 0.75NB2.75S at 10°C/h. Quenching temperature: 1300 °C.

Fig 9. Corrosion potential of pre-oxidized Ni-30Cr vs the temperature in 0.75NB2.75S for two pre-oxidation conditions: 16 h and 64 h at 942°C, temperature increase rate: 50°C/h.

Fig 10. Corrosion potential of pre-oxidized Ni-30Cr (64 h at 942 °C) vs the temperature in 0.75NB2.75S for various immersion temperatures.

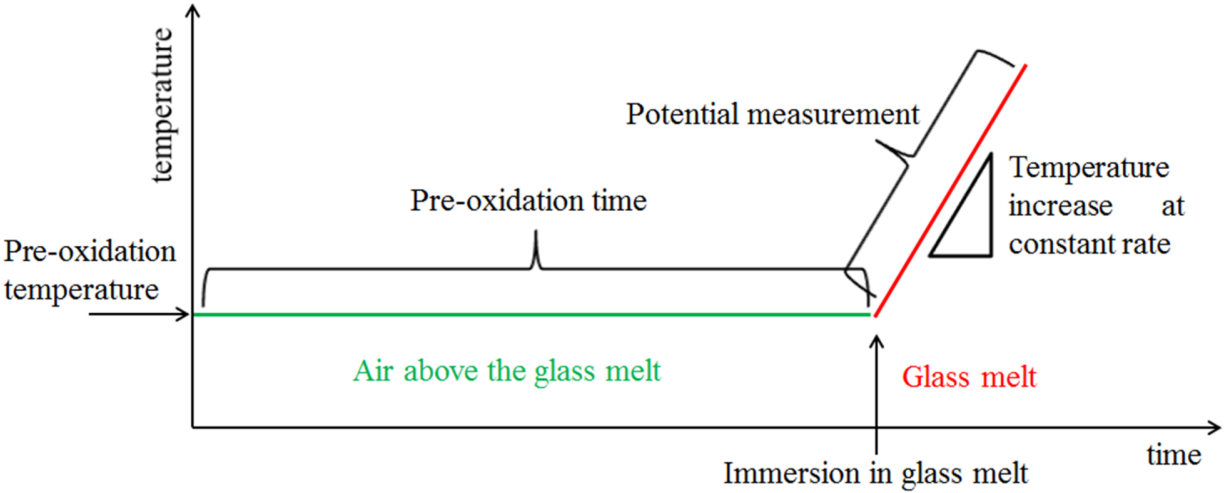
temperature
Potential measurement
Temperature increase at constant rate
Pre-oxidation time
Pre-oxidation temperature
Air above the glass melt
Glass melt
time
Immersion in glass melt

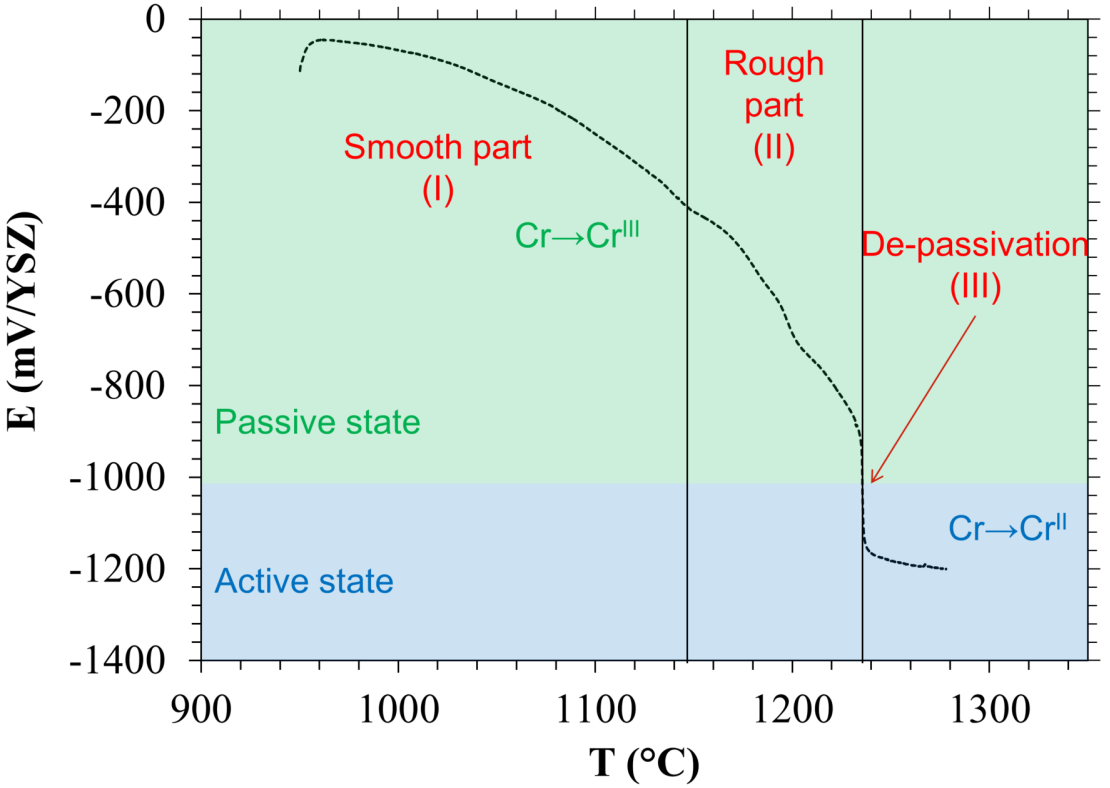
0
-200
-400
-600
-800
-1000
-1200
-1400
E (mV/YSZ)
900
1000
1100
1200
1300
T (°C)
Smooth part
(I)
Rough
part
(II)
De-passivation
(III)
Cr→Cr^III
Cr→Cr^II
Passive state
Active state

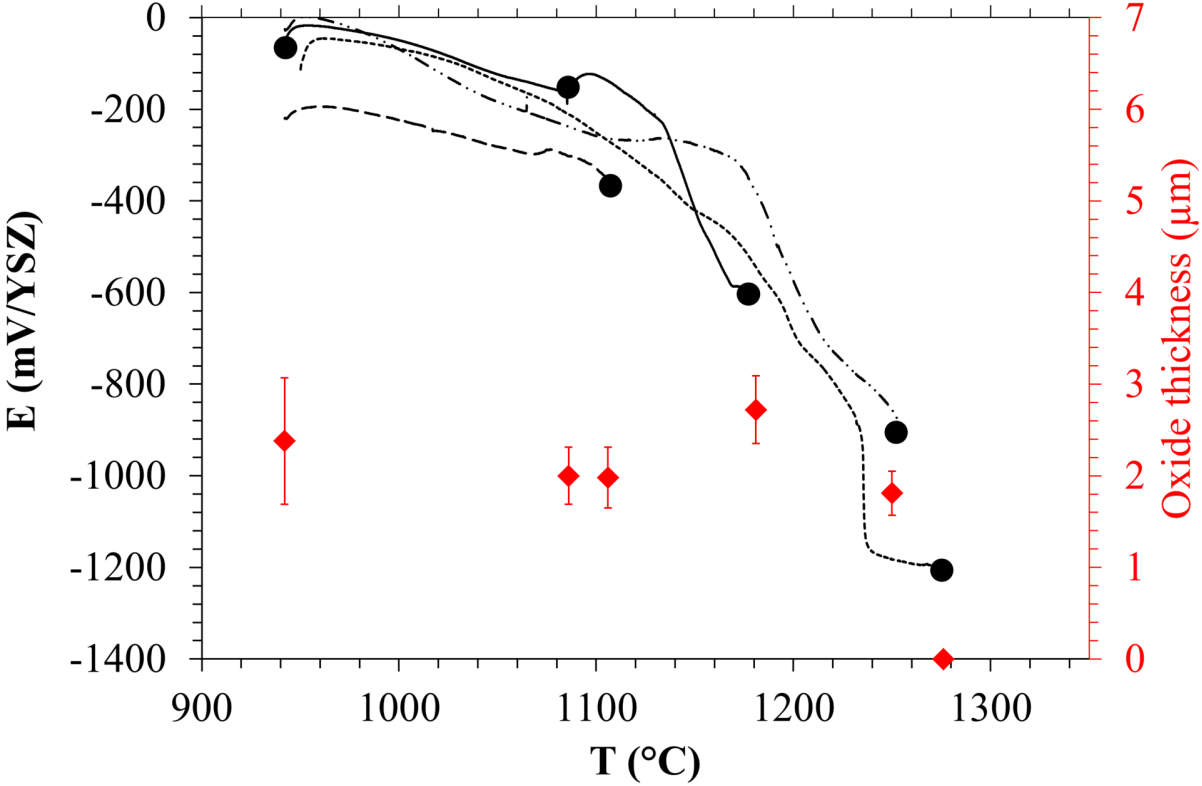
0
-200
-400
-600
-800
-1000
-1200
-1400
E (mV/YSZ)
900
1000
1100
1200
1300
T (°C)
7
6
5
4
3
2
1
0
Oxide thickness (µm)

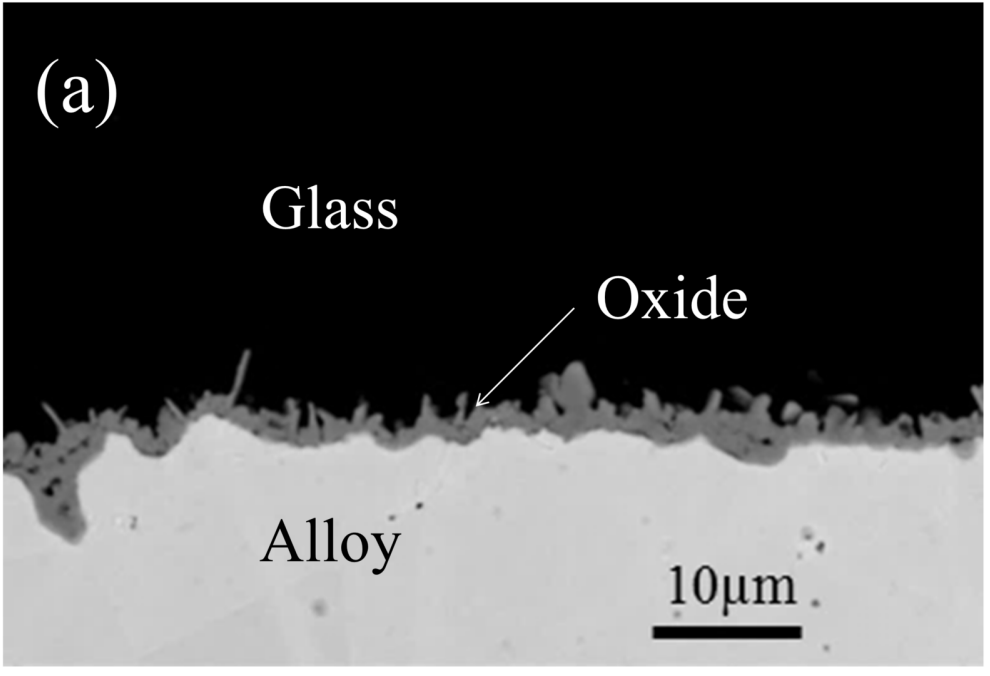
(a)
Glass
Oxide
Alloy
10μm

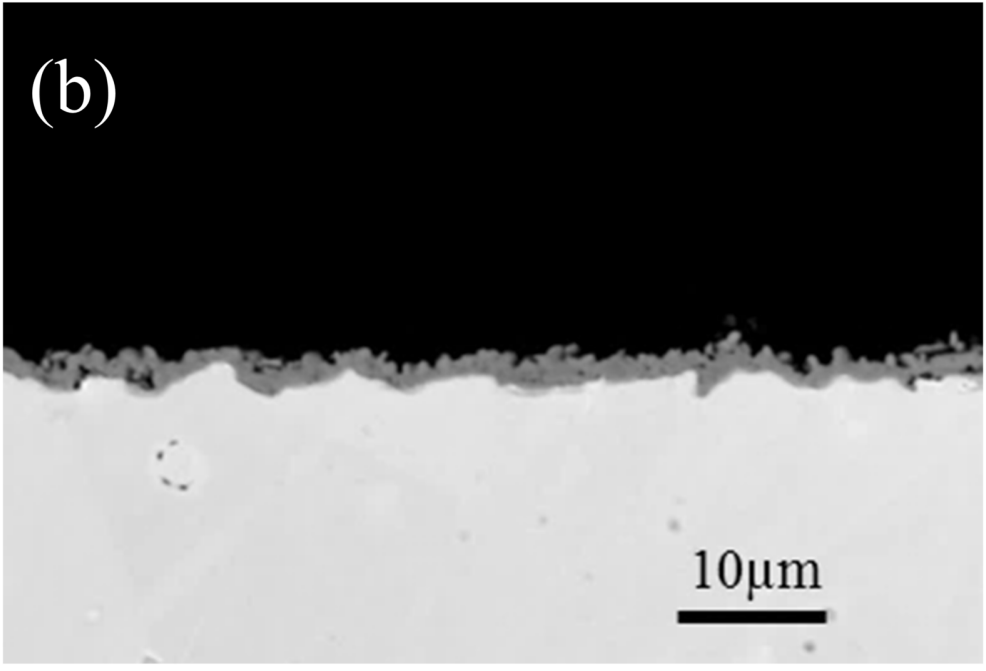
(b)
10μm

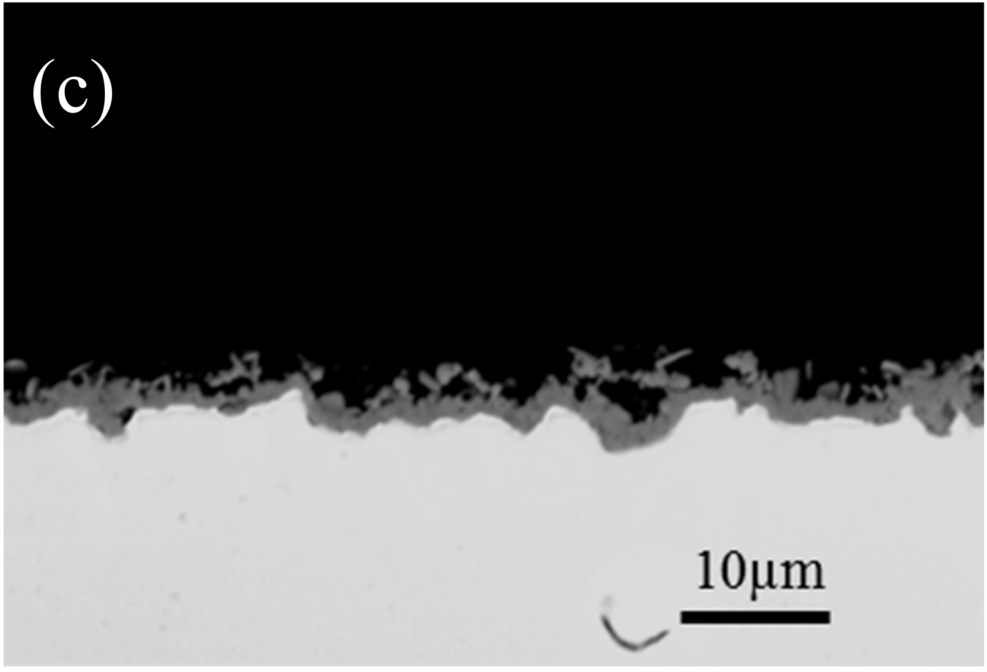
(c)
10μm

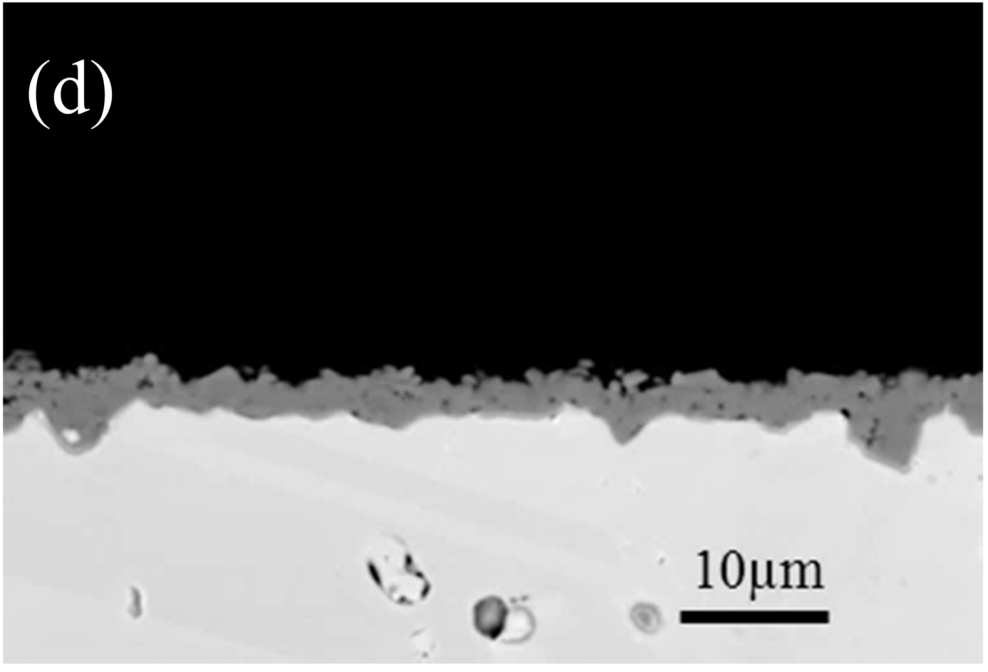
(d)
10μm

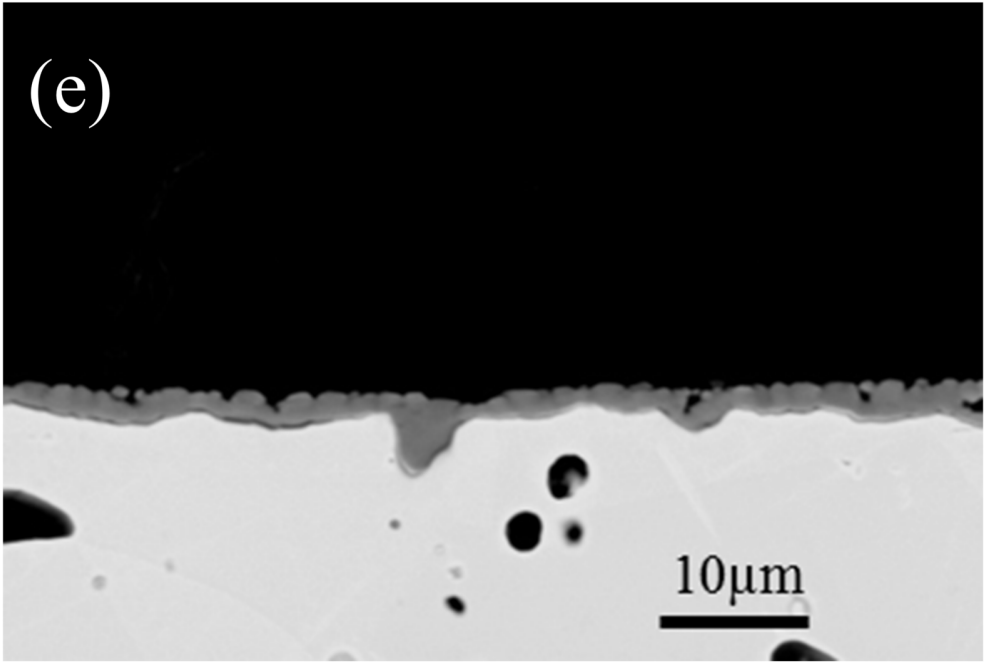
(e)
10μm

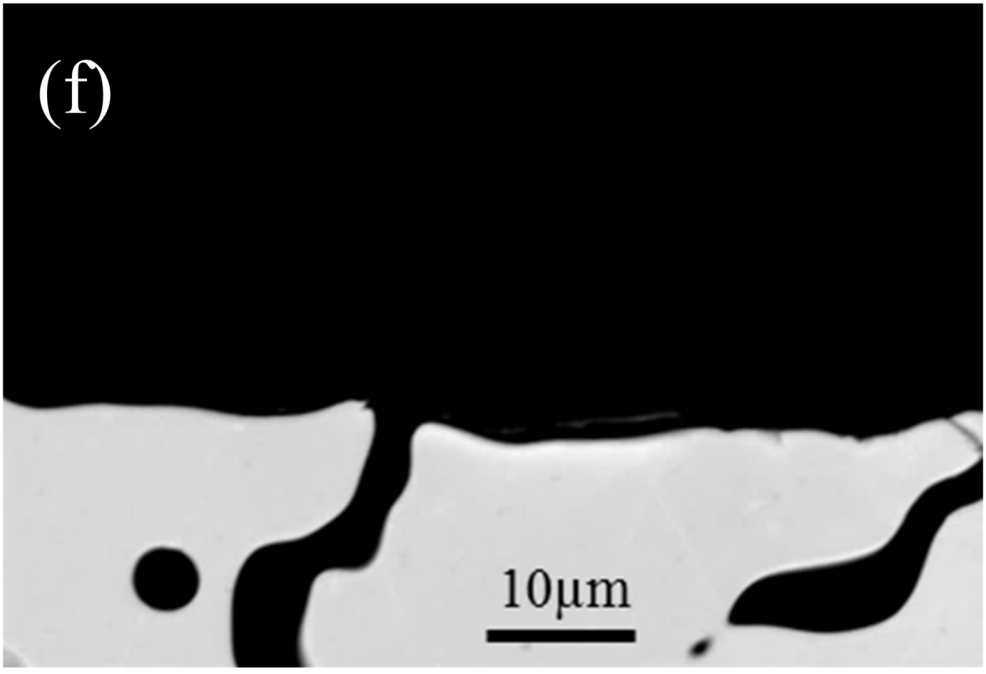
(f)
10μm

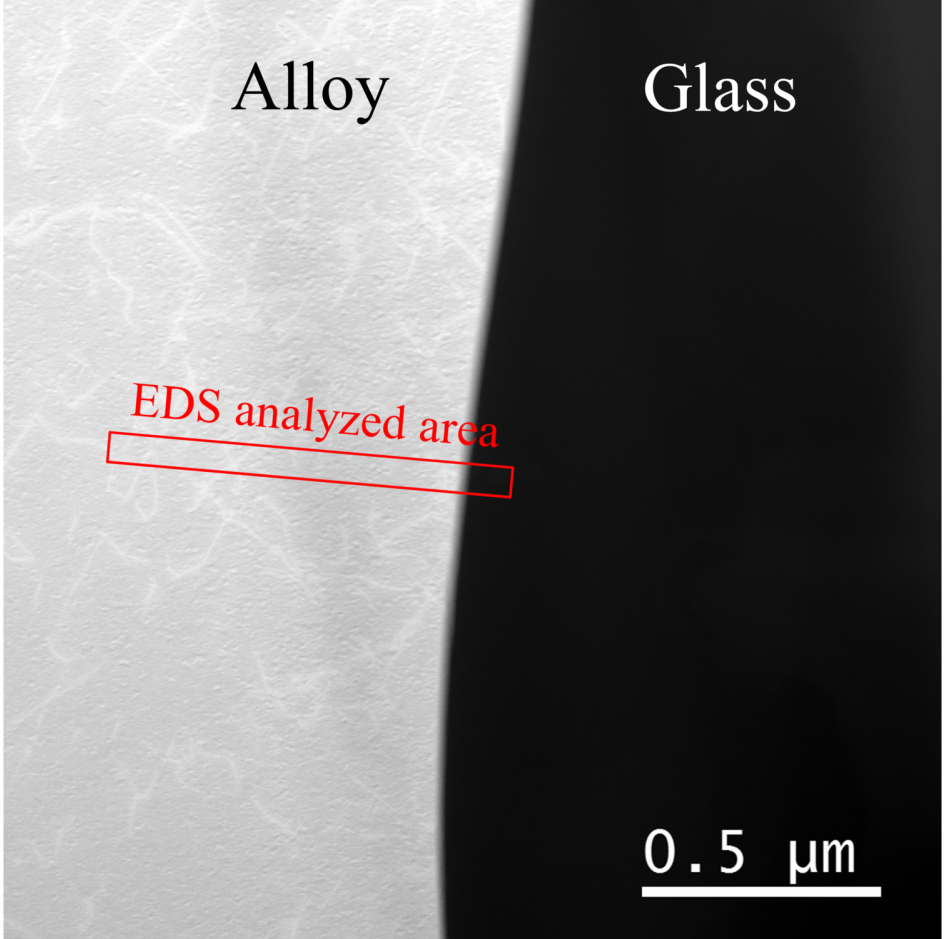
Alloy
Glass
EDS analyzed area
0.5 µm

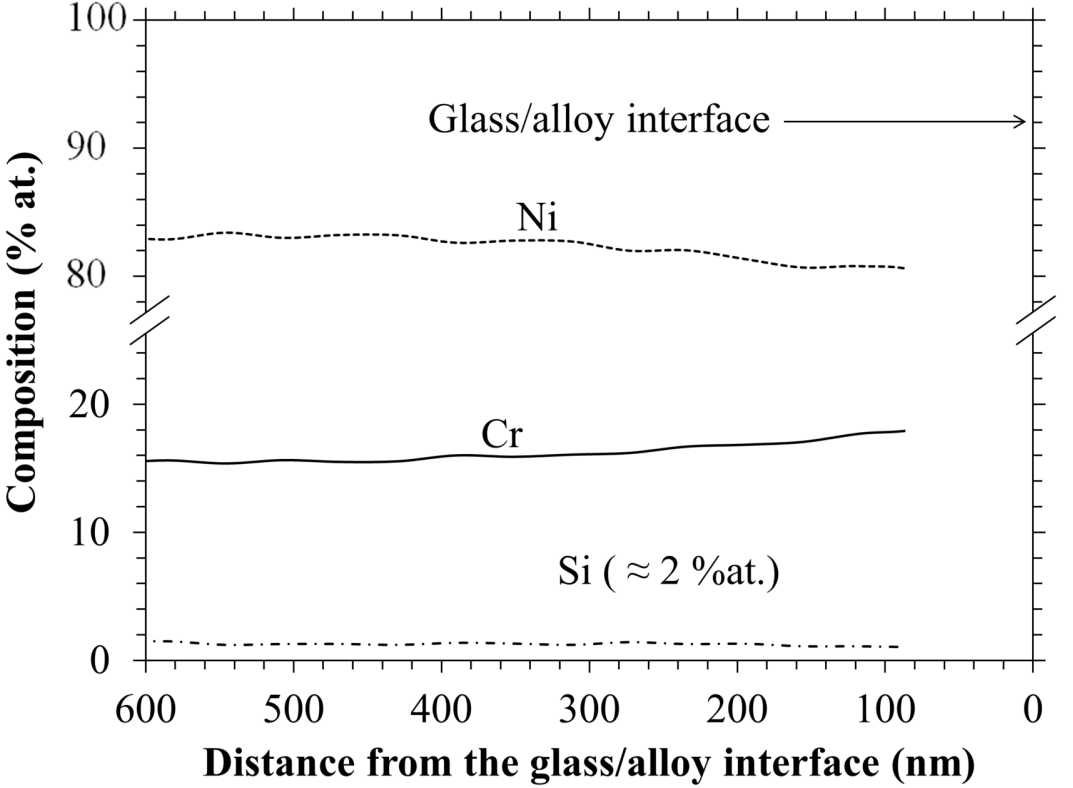
100
90
80
20
10
0
Composition (% at.)
Glass/alloy interface
Ni
Cr
Si (≈ 2 %at.)
600
500
400
300
200
100
0
Distance from the glass/alloy interface (nm)

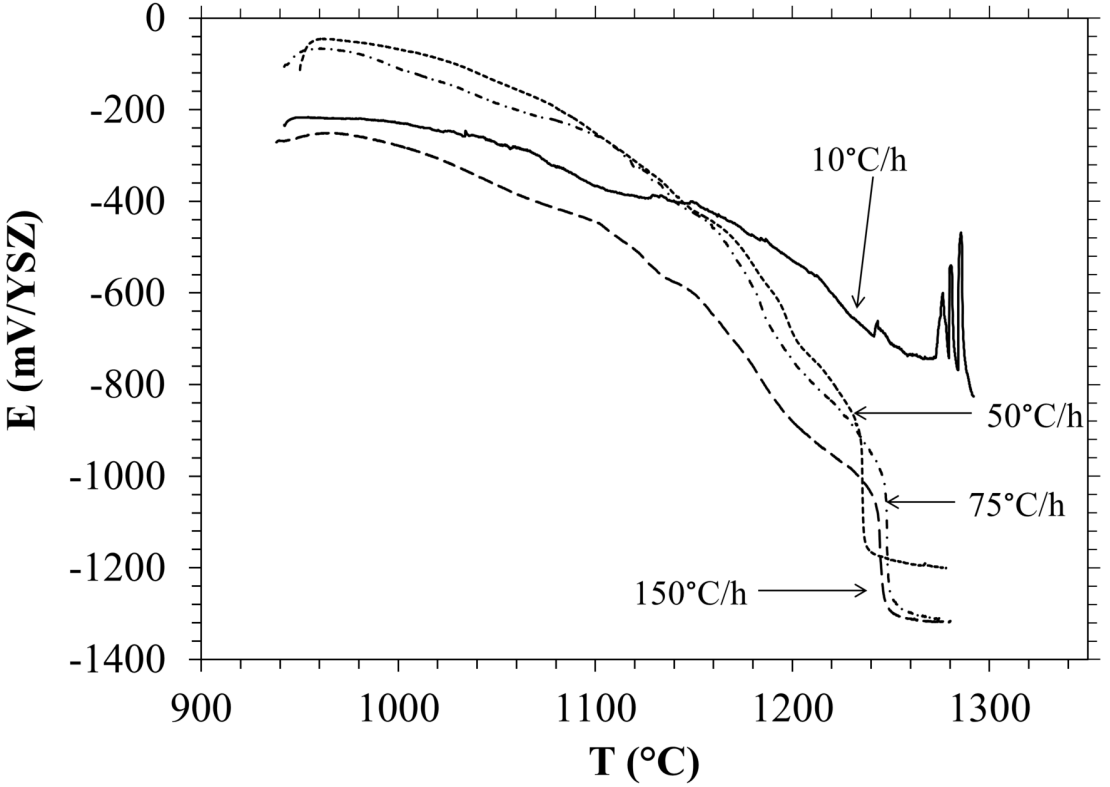
0
-200
-400
-600
-800
-1000
-1200
-1400
E (mV/YSZ)
900
1000
1100
1200
1300
T (°C)
10°C/h
50°C/h
75°C/h
150°C/h

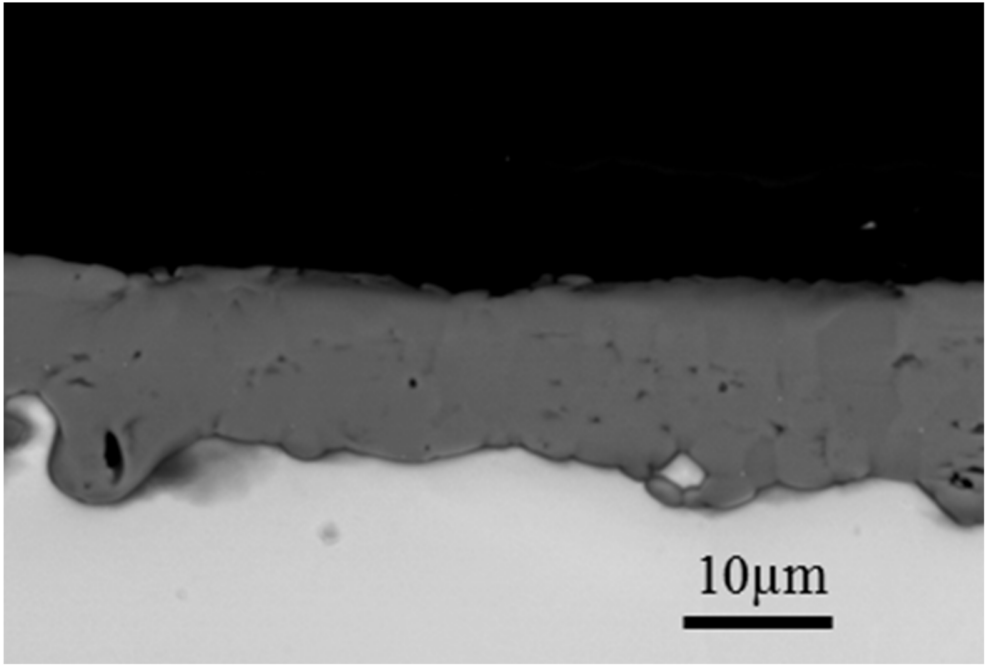
10μm

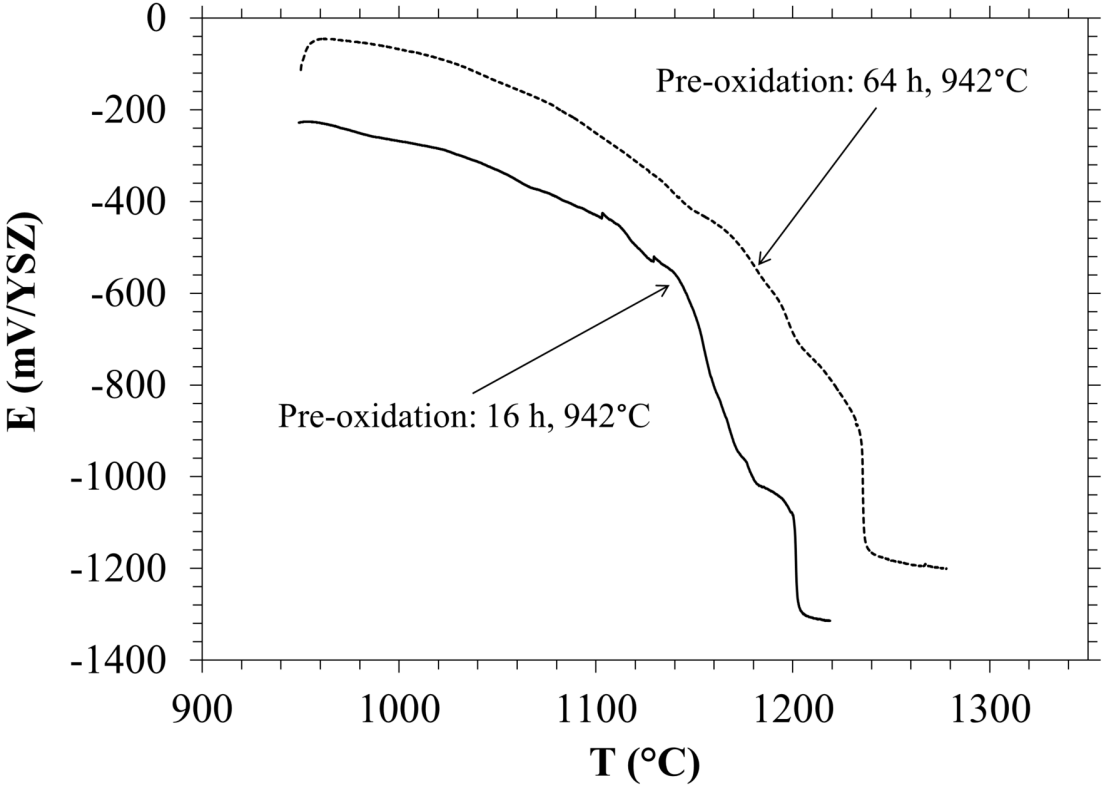
0
-200
-400
-600
-800
-1000
-1200
-1400
E (mV/YSZ)
900
1000
1100
1200
1300
T (°C)
Pre-oxidation: 64 h, 942°C
Pre-oxidation: 16 h, 942°C

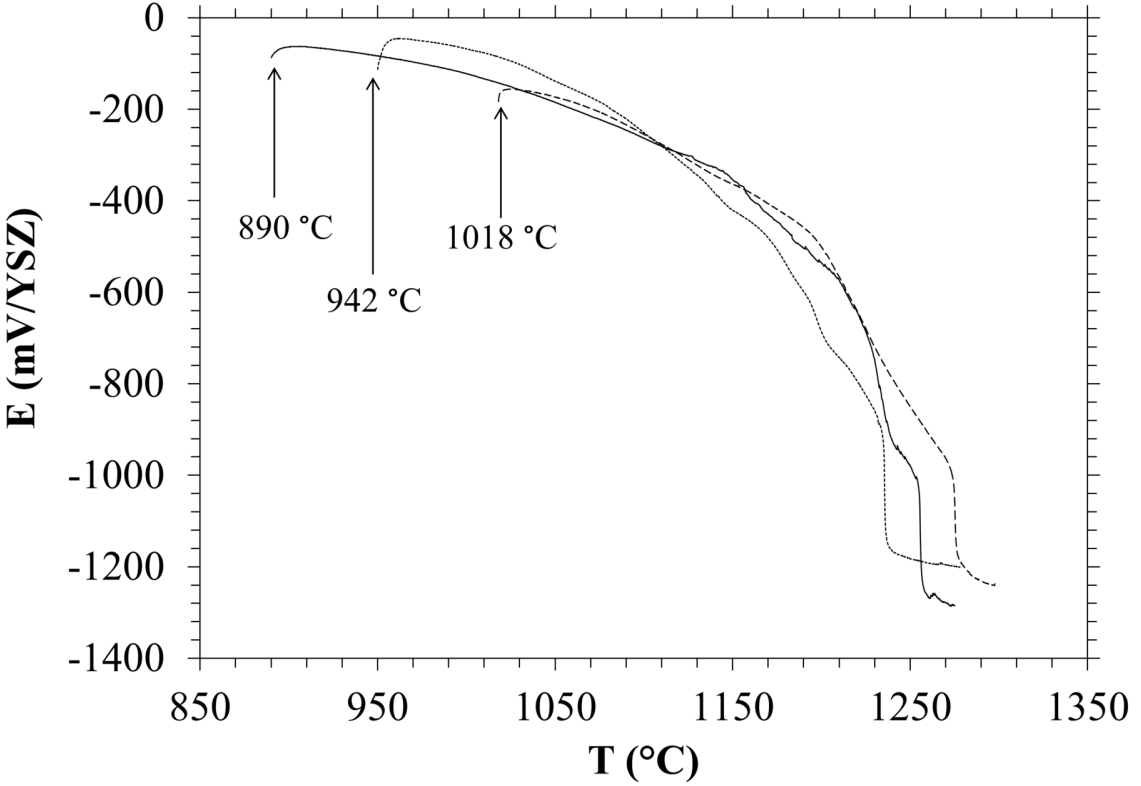
0
-200
-400
-600
-800
-1000
-1200
-1400
E (mV/YSZ)
890 °C
942 °C
1018 °C
850
950
1050
1150
1250
1350
T (°C)

High temperature electrochemical device

Corrosion potential measurement

Electron microscopy characterization

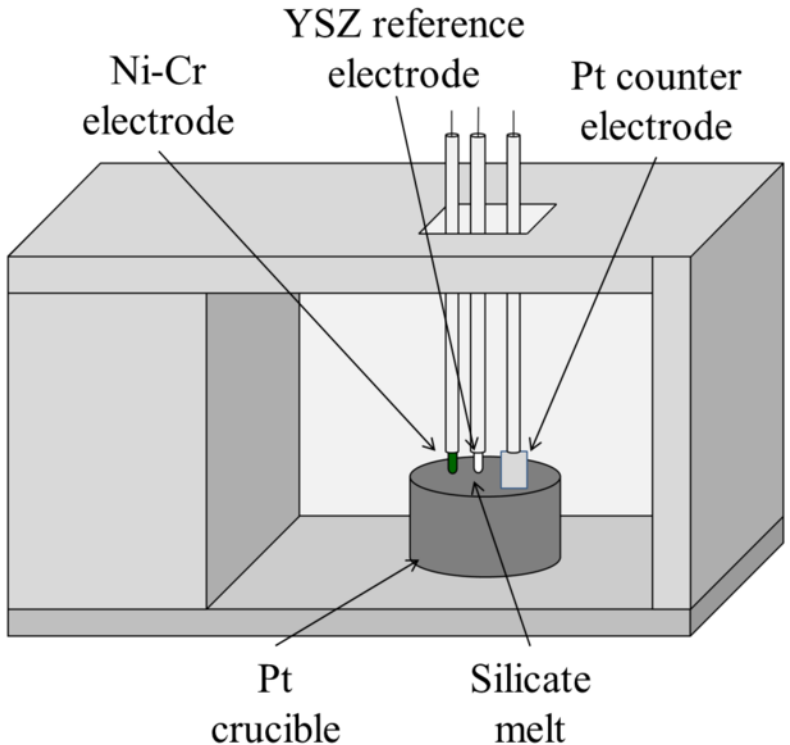

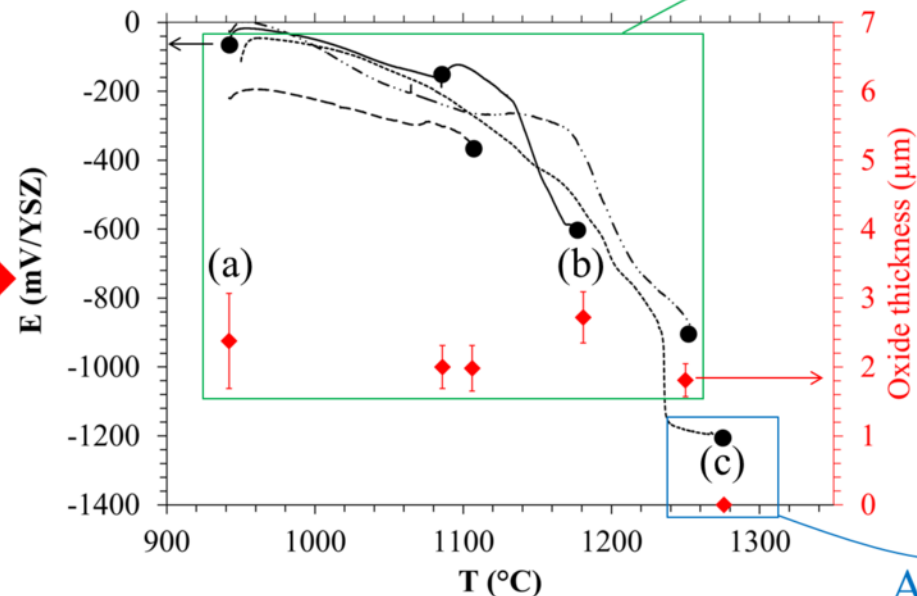

Passive (Protected)

Active (Unprotected)